Journal of Southeast University (English Edition) Vol. 40, No. 2, pp. 176 - 184 June 2024 ISSN 1003—7985

Formation of hysteretic curve similarity indicators based on shape descriptors

Chen Zaixian Xu Yaolong

(Department of Civil Engineering, Harbin Institute of Technology at Weihai, Weihai 264209, China)
(Key Laboratory of Civil Engineering Structure and Disaster Prevention in Universities of Shandong, Harbin Institute of Technology at Weihai, Weihai 264209, China)

Abstract: To develop comprehensive similarity indicators for assessing the fitting degree of hysteretic curves shape descriptors, widely used in image feature extraction, are introduced. A specific process is proposed to delineate the formation of indicators based on these descriptors, enabling the calculation of curve similarity between numerical simulation and experimental data. Following this process, an indicator is devised based on shape context. First, the similarities of the hysteretic loops in the numerical simulation curve are calculated. Subsequently, the weighted sum of these similarities is calculated to derive the similarity of the entire curve. To verify the effectiveness of the indicator, the Bouc-Wen model is utilized to conduct a numerical simulation study. Five parameters of the model are adjusted, resulting in the formation of 51 numerical simulation curves. Similarities of the curve, along with errors in the force peak point, energy dissipation, and stiffness, are calculated. The results show that the absolute values of Spearman's correlation coefficients between similarity and errors all exceed 0.78, which has a strong correlation, thus verifying the feasibility of the indicator and the effectiveness of the process for forming the indicators.

Key words: hysteretic curve; shape descriptor; shape context; Bouc-Wen model; curve similarity

DOI: 10.3969/j.issn.1003-7985.2024.02.008

Hysteretic curves were originally used to describe the behavior of magnetic materials and later found widespread application in mechanics and engineering problems, particularly in earthquake engineering, where nonlinear problems are prevalent[1]. However, currently, there is no globally accepted standard for evaluating the degree of fit between the hysteretic curve obtained from experiments and that obtained from numerical simulations based on experimental conditions. Currently, scholars utilize three main types of evaluation indicators. The first type of indicator is based on errors related to important performance indicators such as peak points, stiffness, and energy dissipation area[2-4], which is not comprehensive. The second type of indicator considers that certain simple structures, such as a brace composed of springs and friction plates connected in series, have clear models. Thus, the evaluation is based on the error of the model parameters[5], but the applicability of the indicators is highly limited. The third type of indicator solely evaluates the fitting degree of two hysteretic curves or skeleton curves[6-8] and is thus subjective. Hence, methods for extracting features from the entire curve and establishing objective indicators are needed.

The advancement of image recognition has led to the proposal of various shape descriptors for extracting invariant features from images. These techniques can also be employed to extract features from hysteretic curves. Among these techniques, image moments, Fourier descriptors, and shape context are widely used. Image moments utilize pixel information, describing image features by computing the weighted sum of gray value, color value, coordinate value, and other pixel attributes. Xiao et al.[9] and Yang et al.[10] introduced fractional-order orthogonal moments and transformed orthogonal moments based on traditional integer-order orthogonal moments, thereby improving their ability to extract local features and resist noise. The Fourier descriptor relies on contours. It involves performing a Fourier transform on the sequence of contour curves, converting curve information into frequency components, and subsequently describing curve features. The introduction of phase-preserving Fourier descriptors and quasi-Fourier descriptors has enhanced the capability of Fourier descriptors to extract invariant features from graphics[11-12]. Shape context, also based on contours, differs from Fourier descriptors. Shape contexts express image information through the coordinate positions of each point relative to other points on the contour. They have found widespread application in several domains, including gesture recognition[13], medical detection[14], and mechanical fault diagnosis[15].

Compared with Fourier descriptors, shape contexts are characterized by a more intuitive geometric interpretation, as frequency components are abstract. Additionally, the precision of Fourier descriptors can be affected by the se-

Received 2023-10-31, **Revised** 2024-04-29.

Biography: Chen Zaixian (1981—), male, doctor, professor, zaixian_chen@sina.com.

Foundation item: The National Science Foundation of China (No. 52078165).

Citation: Chen Zaixian, Xu Yaolong. Formation of hysteretic curve similarity indicators based on shape descriptors[J]. Journal of Southeast University (English Edition), 2024, 40(2): 176 - 184. DOI: 10.3969/j.issn.1003-7985.2024.02.008.

lection of the frequency range. In contrast, the formula for shape contexts is more uniform than that of image moments, as numerous kernel functions are available for image moments. Therefore, in this study, we adopted shape contexts rather than image moments or Fourier descriptors. The application process of shape descriptors for image classification is outlined and a methodology for forming indicators is proposed. Subsequently, the algorithm for shape contexts and an algorithm for a similarity indicator based on the methodology outlined above. Finally, to validate the methodology and the indicator, we employ the Bouc-Wen model for numerical simulation and analyze the similarities of curves under variations in five parameters.

1 Application Process of Shape Descriptors

1.1 Image classification process

Currently, shape descriptors are primarily used for image classification, and their application process is as follows:

1) Collecting images that serve as the subjects of classification. These images encompass static images, such as the CARL face dataset, MPEG-7 dataset, ETH-80 dataset, and Cambridge hand-gesture dataset, as well as images extracted from videos, such as those from the Replay Attack dataset, MSU MFSD dataset, and the DynTex dataset.

2) Preprocessing images to facilitate feature extraction. Preprocessing involves several steps, including denoising, feature enhancement, image segmentation, and contour extraction. Denoising entails removing noise or unwanted artifacts from images. Common denoising methods include smoothing filters, non-local mean denoising, and wavelet denoising. Feature enhancement aims to improve the visual characteristics of an image or highlight useful information by adjusting parameters such as brightness, contrast, and color. Image segmentation divides an image into different parts based on semantic or visual meaning to extract objects or regions of interest for further feature extraction. Contour extraction, commonly utilized for contour-based shape descriptors, employs methods such as Sobel, Prewitt, Roberts operators, and the Canny edge detector.

3) Extracting features using shape descriptors. The features extracted and their format vary according to the descriptor used. For instance, shape context captures the position information of contour points in a histogram format, while the Fourier descriptor analyzes the frequency domain of the contour.

4) Implementing matching algorithms based on extraction results. Simple matching can be conducted using the criterion of minimum distance function value, while more complex matching can be conducted using classifiers such as clustering algorithms, support vector machines, and neural networks.

The entire process has been abridged in the form of a flowchart as shown in Fig. 1.

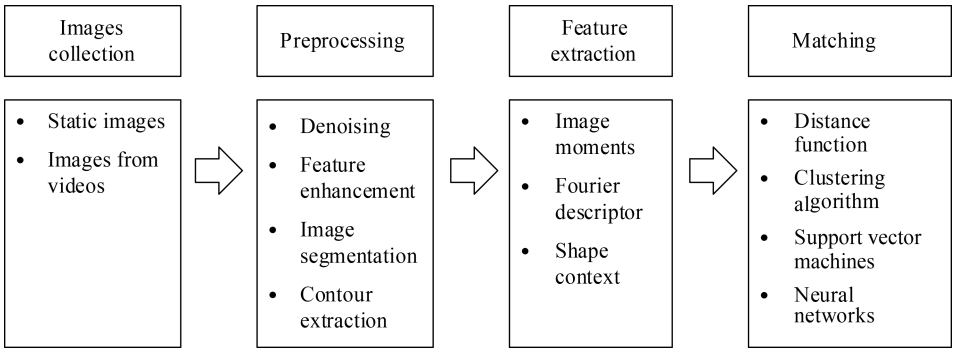

Fig. 1 Flowchart of image recognition based on shape descriptors

1.2 Formation of hysteretic curve similarity indicators

The formation of indicators is similar to the process described in Section 1.1, with three main differences: 1) Algorithms need to adjust to the characteristics of hysteretic curves. 2) The objective is to calculate the matching cost and, subsequently, the similarity without the necessity of classification. 3) Calculation results should be normalized to establish standard indicators.

There are four characteristics of hysteretic curves: 1) A complete hysteresis curve comprises several hysteretic loops and the final segment of the curve, which is not a complete loop. 2) The contours have intersecting parts. 3) The order of the points is fixed and cannot be interchanged. 4) The number, position, and range of coordinate values of the points are determined by the data, varying widely across different experiments.

Therefore, the algorithms for indicators need improvement. First, during preprocessing, it is necessary to accurately divide the curve into hysteretic loops. Then, during matching, it is essential to consider the matching results between all hysteretic loops and conduct a comprehensive evaluation. Contour information should adhere to the sequence of the hysteretic curve to avoid altering the order of points. For applications involving a large volume of data, algorithm optimization is necessary to enhance efficiency. Additionally, the matching process can be appropriately streamlined, but the results from different indicators should fall within a predefined range. If any of the results exceed this range, they should

either be discarded or deemed as indicating insufficient similarity.

The entire process has been summarized in the form of a flowchart in Fig. 2.

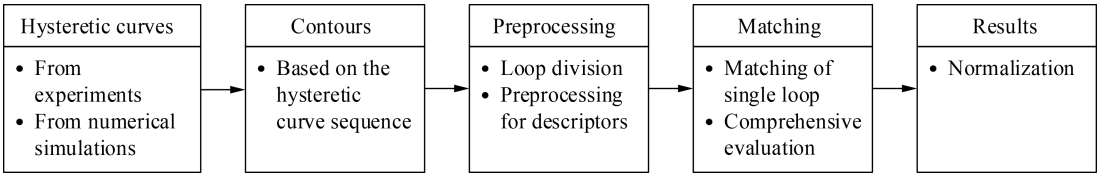

Fig. 2 Flowchart of indicators' formation based on shape descriptors

2 Algorithm

According to the process proposed in Section 1.2, this section introduces shape context, modifies the shape context algorithm, and proposes a method for evaluating the similarity between two hysteretic loops and the similarity between two complete hysteretic curves.

2.1 Algorithm of shape context

Since the inception of the shape context algorithm, there have been specific solutions for 2D and 3D object recognition[16]. The process involves constructing a polar logarithmic coordinate system centered on each contour point and dividing the system evenly into multiple bins based on the logarithm of distance and angle. Subsequently, the count of other points falling into each bin is computed as follows:

$$g_i(r) = \#\{q \neq p_i : (q - p_i) \in \mathrm{bin}(r)\} \tag{1}$$

where $g_i(r)$ is the r-th element of the histogram of the i-th point of the contour; p_i is the i-th point; q is the set of all contour points; $\mathrm{bin}(r)$ is the r-th bin.

Afterward, a histogram is constructed according to the statistical results, where the dimension K represents the total number of bins. For instance, Belongie et al.[16] employed a region set divided into 5 bins based on the logarithm of distance and 12 bins based on angle, resulting in a dimension $K = 60$. Furthermore, the matching cost is calculated, and the cost matrix $\boldsymbol{C}$ is formed between the points of the two contours as follows:

$$C_{i,j} = \frac{1}{2}\sum_{r=1}^{K}\frac{[g_i(r) - h_j(r)]^2}{g_i(r) + h_j(r)} \tag{2}$$

where $C_{i,j}$ is the element in row i and column j of matrix $\boldsymbol{C}$; $h_j(r)$ is the r-th element of the histogram of the j-th point of the second contour.

However, each point can only be matched with one point on the other contour. Therefore, the use of an allocation algorithm, such as the Hungarian algorithm or the shortest augmented path algorithm[16], is necessary to identify the minimum total matching cost and derive the matching result. In cases in which the number of points in the two contours differs, the matrix can be made square by adding "dummy" nodes to one point set, with a constant matching cost assigned to every point.

2.2 Algorithm of an indicator

2.2.1 Similarity algorithm for hysteretic loops

This algorithm is a modification of that described in Section 2.1. Considering that the range of coordinate values is not fixed and that it is difficult to divide bins, the position information of a point is directly represented by its relative coordinates to the centroid. The matching cost between the i-th point of the first loop and the j-th point of the second loop is calculated as follows:

$$C_{i,j} = \sqrt{(x_{1,i} - x_{2,j})^2 + (y_{1,i} - y_{2,j})^2} \tag{3}$$

where $(x_{1,i}, y_{1,i})$ is the coordinate of the i-th point of the first loop relative to its centroid, and $(x_{2,j}, y_{2,j})$ is the coordinate of the j-th point of the second loop relative to its centroid.

The matching is resolved using the Hungarian algorithm. For cases in which the number of points in the two loops differs, where L_1, containing N_1 points, denotes the loop with fewer points, and L_2, containing N_2 points, denotes the loop with more points, the matching cost for the i'-th point $(p_{i'})$ of the additional $N_2 - N_1$ points in L_2 can be calculated as follows:

$$D_{i'} = \frac{|\overrightarrow{p_{i'}p'} \times \overrightarrow{p_{i'}p''}|}{|\overrightarrow{p'p''}|} \tag{4}$$

where p' is the point (in L_1) matched by the previous matchable point (in L_2) of $p_{i'}$, and p'' is the point (in L_1) matched by the next matchable point (in L_2) of $p_{i'}$. If one of p' and p'' is not found, its coordinates are set as $(0,0)$ (coordinates of the centroid). The equation calculates the distance from $p_{i'}$ to the straight line connecting p' and p''. Then, the similarity of the second loop relative to the first loop S can be calculated as follows:

$$S = 1 - \frac{\sum_{i=1}^{N} C_{i,j_i} + \sum_{i'=1}^{M-N} D_{i'}}{r_{1,\mathrm{mean}} N_2} \tag{5}$$

where j_i is the sequence number of the point in the second loop that matches the i-th point in the first loop, and $r_{1,\mathrm{mean}}$ is the mean distance from all points of the first loop to its centroid. It is easy to find that $S \leqslant 1$. When the two curves are exactly the same, $S = 1$.

2.2.2 Similarity algorithm for hysteretic curve

A complete hysteretic curve comprises several hyster-

etic loops and the final segment of the curve, which is not a complete loop. Under reasonable loading conditions, the final segment that cannot form a complete loop often does not exist or accounts for a small proportion. Thus, this segment is typically ignored in the evaluation of the similarity of the hysteretic curve. The objective of this algorithm is to assess the similarity between the curves obtained from the experiment and the numerical simulation. Therefore, the operating conditions of the two curves should be identical, leading to an equal number of loops in most cases. The similarity of the first loop of the curve from numerical simulation relative to the first loop of the curve from the experiment is calculated as S_1. Then, the similarity of the second loop of the curve from numerical simulation relative to the second loop of the curve from the experiment is calculated as S_2, and so forth. The similarity of all loops in the curve from numerical simulation is determined. The overall similarity of the curve from numerical simulation S_{all} can then be derived by computing the weighted sum of these similarities:

$$S_{\text{all}} = \sum_{i=1}^{M} a_i S_i \tag{6}$$

where M is the number of loops; a_i is the weight coefficient of i-th loop's similarity, which needs to meet the following conditions:

$$\sum_{i=1}^{M} a_i = 1 \tag{7}$$

For this paper, $a_1 = a_2 = \ldots = a_M = 1/M$.

However, the varying dimensions and value ranges of force and displacement affect the similarity calculated by Eq. (5) differently. For instance, when the force value range is large and the displacement value range is small, although the displacement deviation between the two curves might be significant, the similarity could appear very large because the dissimilarity of displacement has a minor negative impact on the similarity. To ensure that force and displacement contribute equally, their value ranges need adjustment. For each point's displacement in the two curves, the following processing is performed:

$$u_i' = \frac{\max(F_{\text{exp}}) - \min(F_{\text{exp}})}{\max(u_{\text{exp}}) - \min(u_{\text{exp}})} u_i \tag{8}$$

where u_i' is the displacement of the i-th point after processing; u_i is the displacement of the i-th point before processing; u_{exp} is the displacement of all points in the curve from the experiment; F_{exp} is the force of all points in the curve from the experiment.

3 Experiments and Results

3.1 Model and parameters

To validate the indicator through numerical simulation, this section employs the Bouc-Wen model for variable parameter analysis. First, the equation of motion for a single-degree-of-freedom system, as depicted in Fig. 3, can be formulated as follows:

$$m\ddot{u} + c\dot{u} + \alpha k u + (1-\alpha) k z = F(t) \tag{9}$$

where u is the displacement of mass m; c is the linear viscous damping coefficient; k is the initial stiffness; α is stiffness ratio; z is the hysteretic displacement; and $F(t)$ is the time-dependent forcing function. In the equation, $\alpha k u$ is the linear restoring force; $(1-\alpha) k z$ denotes the hysteretic restoring force; their sum yields the nondamping restoring force. The relationship between z and u is as follows:

$$\dot{z} = h(z) \frac{A\dot{u} - \nu(\beta |\dot{u}| |z|^{n-1} z + \gamma \dot{u} |z|^n)}{\eta} \tag{10}$$

where A denotes the tangent stiffness; $h(z)$ is the pinching function; β, γ, and n are hysteretic shape parameters; ν and η are strength and stiffness degradation parameters, respectively, which are the functions of total hysteretic energy as shown in the following expressions:

$$\nu(\varepsilon) = 1 + \delta_\nu \varepsilon \tag{11}$$

$$\eta(\varepsilon) = 1 + \delta_\eta \varepsilon \tag{12}$$

where δ_ν and δ_η are the designated rates of strength and stiffness degradation, respectively. Hysteretic energy ε is the energy absorbed by the hysteretic element, and it can be expressed as

$$\varepsilon(t) = (1-\alpha) \omega_0^2 \int_0^t z(u, t) \dot{u}(t) \, \mathrm{d}t \tag{13}$$

where ω_0 is the natural frequency of the preyield system, $\omega_0 = \sqrt{k/m}$. To solve the differential equations, the fourth-order Runge-Kutta method is used[17].

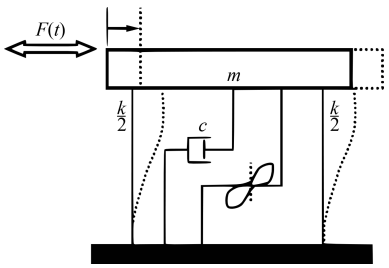

Fig. 3 Schematic model of a single-degree-of-freedom hysteretic system

To determine the relationship between the alteration of the curve and the variation in similarity, a curve is constructed under specific parameter conditions as the experimental curve. Subsequently, each parameter is individually adjusted to generate several curves from numerical simulation.

The initial parameter conditions are detailed in Table 1, where ξ represents the damping ratio. As parameter A is somewhat redundant because both hysteretic stiffness

and hysteretic force can be varied by the stiffness ratio and hysteresis shape parameters[18], it is set to unity. The calculation of $h(z)$ is complex, which could lead to an increase in the number of parameters. Currently, its parameters and calculation methods may be simplified[19]. Hence, this paper does not consider the pinching effect, and $h(z)$ is set to 1. The loading condition is illustrated in Fig. 4. The loading cycle spans 10 s; the peak force of the first cycle is 150 kN, and the force for each subsequent cycle increases by 10 kN. The total loading time is 100 s, with a sampling frequency of 50 Hz. The range of parameter changes is provided in Table 2. Considering that ambient excitation may influence the dynamic characteristics of the structure[20], this paper assumes a steady environment during the loading process.

Table 1 Initial parameter conditions

Parameter	Value	Parameter	Value
m/kg	1 200	k/(kN·m^{-1})	7 110
ξ	0.02	n	2
γ	500	α	0.050
β	500	δ_ν	0.050
δ_η	0.02	A	1

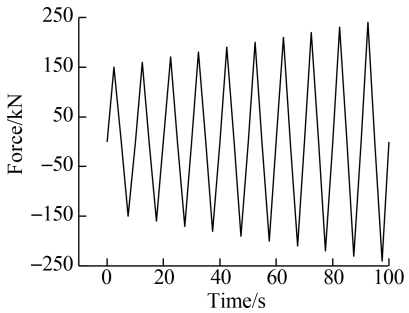

Fig. 4 Loading path

Table 2 Variation range of every parameter

Parameter	Minimum	Middle	Maximum
γ	250	500	750
β	250	500	750
δ_ν	0.025	0.050	0.075
δ_η	0	0.02	0.04
α	0.025	0.050	0.075

Existing articles provide related descriptions regarding the impact of changes in various parameters of the Bouc-Wen model on the curve shape[18, 21–22]. Fig. 5 illustrates the shape of curves when each parameter takes on the minimum, middle, and maximum values, as specified in Table 2. Parameters such as β, γ, and δ_ν can influence the fullness of hysteretic loops, while δ_η affects the shape of hysteretic loops, primarily at the corners. Parameter α can alter the angle of loops.

3.2 Parameter variation and results

For each parameter, 11 values evenly spaced are selected within its range, including the minimum and maximum values, and 11 curves are developed accordingly.

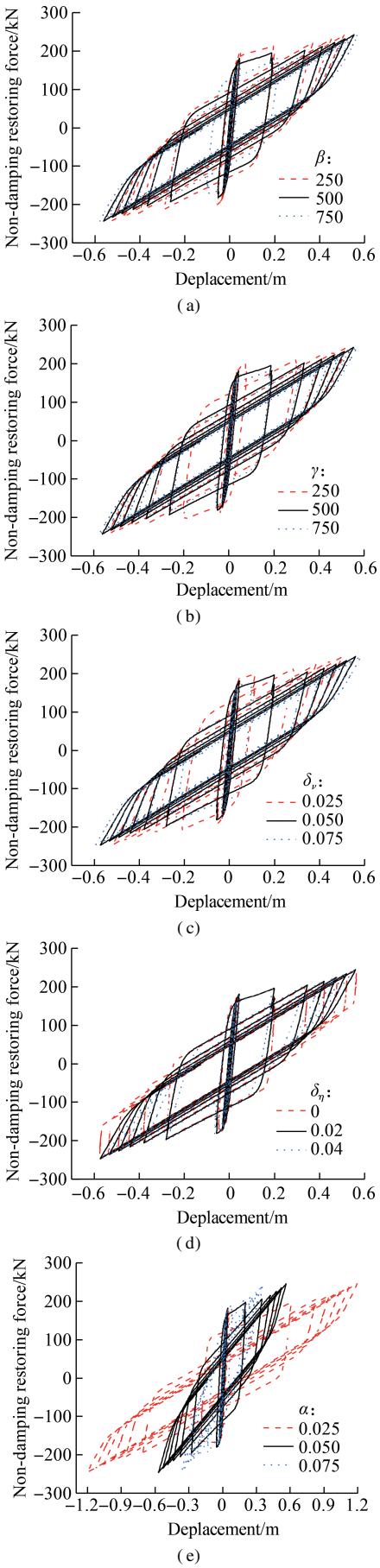

Fig. 5 Curves under different parameters. (a) β; (b) γ; (c) δ_ν; (d) δ_η; (e) α

Apart from the curve generated by the middle value, which perfectly aligns with the curve from the experiment, the other curves differ. Therefore, a total of 51 distinct curves are generated, all derived from numerical simulation. The similarities of these curves relative to the experimental curve are individually calculated (see Fig. 6). The greater the parameters change compared with the middle value, the smaller the similarity. The magnitude of parameter changes correlates with the dissimilarity of the curves, thereby indicating that this algorithm can effectively reflect the dissimilarity of the curves.

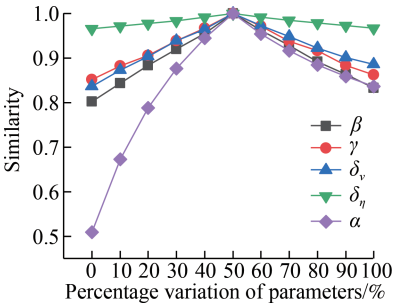

Fig. 6 Relationship between similarity results and variation of each parameter

For hysteretic curves, particular emphasis is often placed on performance indicators such as the peak point, energy dissipation capacity, and stiffness. Traditional comparisons of hysteretic curves frequently focus on these aspects. Hence, investigating whether similarity can accurately reflect the degree of similarity in these respects is essential. This paper utilizes the relative average error of displacement at the force peak point (ED), the energy dissipation area (EA), and the secant stiffness (ES) to represent these indicators. The relative average error is calculated as

$$e = \frac{\sum_{j=1}^{Q} \left| \frac{A_{\text{num},j} - A_{\text{exp},j}}{A_{\text{num},j}} \right|}{Q} \tag{14}$$

where e is the relative average error of the indicator; $A_{\text{num},j}$ is the indicator value of the j-th loop in the curve from numerical simulation; $A_{\text{exp},j}$ is the indicator value of the j-th loop in the curve from numerical simulation; Q is the number of loops. Secant stiffness is calculated according to JGJ/T 101—2015[23]:

$$K_j = \frac{|+F_j| + |-F_j|}{|+X_j| + |-X_j|} \tag{15}$$

where K_j is the secant rigid of the j-th loop, $|+F_j|$, $|-F_j|$ are restoring force values at the peak points of the forward and reverse of the j-th loop, and $|+X_j|$, $|-X_j|$ are displacement values at the peak points of the forward and reverse of the j-th loop, respectively.

The errors resulting from changes in each parameter are depicted in Fig. 7. Errors are all zero when parameters assume their respective median values. As a parameter deviates from the median, the errors increase, with varying rates depending on the parameter. Moreover, in most cases, the error increase rate when a parameter is less than the median differs from the rate when the parameter is greater than the median.

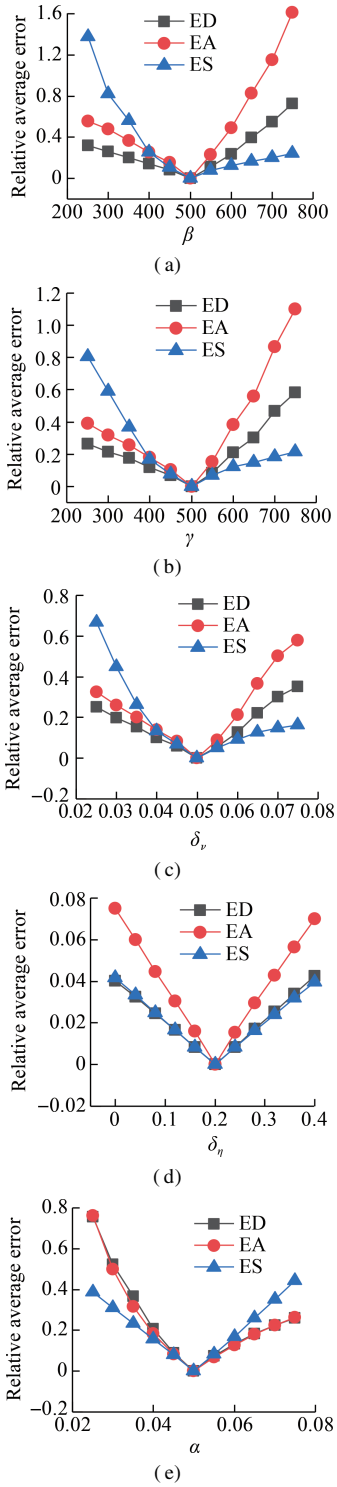

Fig. 7 Relationship between errors and each parameter. (a) β; (b) γ; (c) δ_ν; (d) δ_η; (e) α

The relationship between similarity and errors resulting from changes in each parameter is illustrated in Fig. 8. When the similarity is 1, the errors are 0. As the similar-

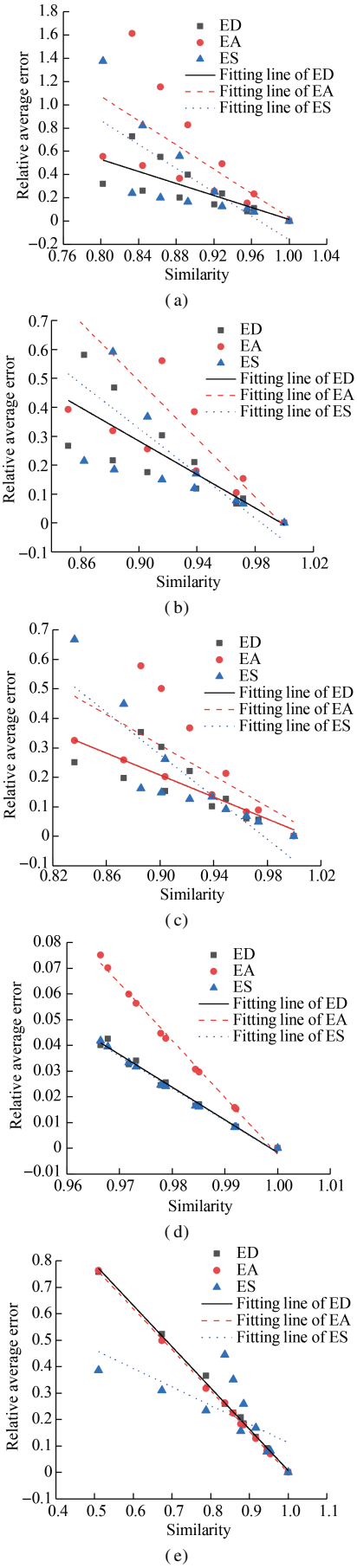

Fig. 8 Similarity and errors when each parameter changes. (a) β; (b) γ; (c) δ_ν; (d) δ_η; (e) α

ity increases, the errors of the three indicators exhibit a downward trend. According to the fitted lines between errors and similarity, a negative correlation exists between errors and similarity. However, in some instances, the results exhibit significant discreteness and deviate noticeably from the line. This disparity is attributed to the varying correlation when a parameter is less than the median compared to when the parameter is greater than the median, as indicated by the relationships shown in Figs. 6 and 7.

The Spearman's correlation coefficients between similarity and errors are shown in Table 3. When a certain parameter changes within a range smaller or larger than the median value, a notable negative correlation exists between the similarity and errors of the three indicators. Although the correlation weakens across the entire range, the absolute values of Spearman' s correlation coefficients between similarity and the three indicators exceed 0. 78. This indicates a significant correlation between their ranks. Overall, the similarity indicator can effectively reflect the outcomes of traditional indicators with just one calculation. Moreover, the algorithm evaluates based on all data points, whereas traditional indicators assess only a portion of them. These results underscore the comprehensiveness of the indicator.

Table 3 Spearman's correlation coefficients between similarity and errors

Parameter	Displacement at the force peak point	Energy dissipation area	Secant stiffness
β	−0. 827 3	−0. 781 8	−0. 872 7
γ	−0. 845 5	−0. 809 1	−0. 927 3
δ_ν	−0. 872 7	−0. 790 9	−0. 963 6
δ_η	−0. 963 6	−1. 000 0	−1. 000 0
α	−1. 000 0	−1. 000 0	−0. 827 3

4 Conclusions

1) A process for constructing hysteretic curve similarity indicators based on shape descriptors is proposed. An indicator and its algorithm are developed accordingly. Numerical simulation results demonstrate the algorithm' s efficacy in evaluating the fitting degree between hysteretic curves from numerical simulations and those from experiments. The feasibility of the indicator validates the effectiveness of the process.

2) Alterations are made to five parameters of the Bouc-Wen model, resulting in the development of 51 distinct curves to assess the indicator. The greater the change in each parameter, the lower the similarity of the curve relative to the original curve. These findings illustrate the indicator' s ability to reflect the similarity of parameters and, subsequently, the similarity of curves.

3) After parameter alteration, the similarities of hysteretic curves relative to the original curve exhibit a negative correlation with the relative average errors of dis-

placement corresponding to the force peak point, the energy dissipation area, and the secant stiffness. Moreover, the absolute values of Spearman's correlation coefficients are all greater than 0.78. This correlation demonstrates that the indicator can effectively reflect the similarity of the peak point, energy dissipation capacity, and stiffness, making it a comprehensive indicator.

References

[1] Hernández-Montes E, Carbonell-Márquez J F, Gil-Martín L M. The energy-balanced hysteretic curve for dynamic loading[J]. *Engineering Structures*, 2021, **229**: 111600. DOI: 10.1016/j.engstruct.2020.111600.

[2] Xing K D, Lin Y Z, Li M H, et al. Analysis on seismic performance of precast segmental concrete-filled double-skin steel tube columns[J]. *Journal of Southeast University* (*Natural Science Edition*), 2023, **53**(2): 305−314. DOI: 10.3969/j.issn.1001-0505.2023.02.014. (in Chinese)

[3] Zeng Z Y, Miao C Q, Sun C Z. Seismic behavior of columns with PVA fiber high strength reinforced concrete in potential plastic region[J]. *Journal of Southeast University* (*Natural Science Edition*), 2023, **53**(2): 242−251. DOI: 10.3969/j.issn.1001-0505.2023.02.007. (in Chinese)

[4] Jin H J, Sun F F, Li G Q, et al. Seismic performance of modular buckling-restrained steel shear walls[J]. *Journal of Southeast University* (*Natural Science Edition*), 2024, **54**(1): 25−35. DOI: 10.3969/j.issn.1001-0505.2024.01.004. (in Chinese)

[5] Xu L H, Yao S Q. Experimental study and finite element simulation on hysteretic performance of self-centering energy dissipation brace[J]. *Journal of Building Structures*, 2018, **39**(11): 158−165. DOI: 10.14006/j.jzjgxb.2018.11.018. (in Chinese)

[6] Wu Y F, Li A Q, Wang H, et al. Numerical simulation and analysis of hysteretic behavior of RC two-columned pier[J]. *Journal of Southeast University* (*Natural Science Edition*), 2015, **45**(4): 776−781. DOI: 10.3969/j.issn.1001-0505.2015.04.028. (in Chinese)

[7] Pellecchia D, Vaiana N, Spizzuoco M, et al. Axial hysteretic behaviour of wire rope isolators: Experiments and modelling[J]. *Materials & Design*, 2023, **225**: 111436. DOI: 10.1016/j.matdes.2022.111436.

[8] Wang W Q, Wang J F, Guo L, et al. Development of hysteretic model for LEM-filled CFS shear walls under cyclic loading[J]. *Engineering Structures*, 2023, **280**: 115651. DOI: 10.1016/j.engstruct.2023.115651.

[9] Xiao B, Li L P, Li Y, et al. Image analysis by fractional-order orthogonal moments[J]. *Information Sciences*, 2017, **382**: 135−149. DOI: 10.1016/j.ins.2016.12.011.

[10] Yang J W, Zeng Z Z, Kwong T, et al. Local orthogonal moments for local features[J]. *IEEE Transactions on Image Processing*: *A Publication of the IEEE Signal Processing Society*, 2023, **32**: 3266−3280. DOI: 10.1109/TIP.2023.3279525.

[11] Sokic E, Konjicija S. Shape description using phase-preserving Fourier descriptor[C]//2015 *IEEE International Conference on Multimedia and Expo* (*ICME*). Turin, Italy, 2015: 1−6.

[12] Yang C Y, Lu L, Zhang L, et al. Quasi Fourier descriptor for affine invariant features[C]//*International Conference on Intelligent Computing*. Cham, Switzerland: Springer, 2022: 245−257.

[13] Qaisar S M, Krichen M, Mihoub A. Hand gesture recognition based on shape context analysis[C]//2021 1*st International Conference on Artificial Intelligence and Data Analytics* (*CAIDA*). Riyadh, Saudi Arabia, 2021: 127−131.

[14] Dias J P, Bhuiyan A, Shamim N. Diagnostic of injury risk in the anterior cruciate ligament based on shape context description of the intercondylar Notch curvature[J]. *Journal of Engineering and Science in Medical Diagnostics and Therapy*, 2022, **5**(2): 021001. DOI: 10.1115/1.4053063.

[15] Wang D Y, Liu H Z, Ren H. Fault diagnosis of sucker rod pumping system based on matching method of shape context[J]. *Journal of China University of Petroleum* (*Edition of Natural Sciences*), 2019, **43**(4): 159−165. DOI: 10.3969/j.issn.1673-5005.2019.04.019. (in Chinese)

[16] Belongie S J, Malik J, Puzicha J. Shape context: A new descriptor for shape matching and object recognition[C]// 14*th Annual Neural Information Processing Systems Conference* (*NIPS*). Denver, CO, USA, 2000: 831−837.

[17] Zhao L, Tu T G, Ding S W, et al. Simulation study of new buckling restraint bracing based on Bayesian optimization algorithm to identify the parameters of modified Bouc-Wen model[J]. *Advances in Civil Engineering*, 2023, **2023**: 4331735. DOI: 10.1155/2023/4331735.

[18] Sengupta P, Li B. Modified Bouc-Wen model for hysteresis behavior of RC beam-column joints with limited transverse reinforcement[J]. *Engineering Structures*, 2013, **46**: 392−406. DOI: 10.1016/j.engstruct.2012.08.003.

[19] Wei K L, Xu Y Z. Hysteretic model and parameter identification of RC bridge piers based on a new modified Bouc-Wen model[J]. *Structures*, 2022, **43**: 1766−1777. DOI: 10.1016/j.istruc.2022.07.049.

[20] Zheng W Z, Wang H, Du Y F, et al. Temperature effect of time-varying modal frequency of base-isolated structure under ambient excitation[J]. *Journal of Southeast University* (*Natural Science Edition*), 2017, **47**(5): 999−1005. DOI: 10.3969/j.issn.1001-0505.2017.05.025. (in Chinese)

[21] Liberatore D, Addessi D, Sangirardi M. An enriched Bouc-Wen model with damage[J]. *European Journal of Mechanics-A/Solids*, 2019, **77**: 103771. DOI: 10.1016/j.euromechsol.2019.04.006.

[22] Wong C W, Ni Y Q, Ko J M. Steady-state oscillation of hysteretic differential model. Ⅱ: Performance analysis[J]. *Journal of Engineering Mechanics*, 1994, **120**(11):

2299 – 2325. DOI: 10. 1061/(asce) 0733-9399 (1994) 120: 11(2299).
[23] Ministry of Housing and Urban-Rural Development of the People's Republic of China. Specification for seismic test of buildings: JGJ/T 101—2015[S]. Beijing: China Architecture & Building Press, 2015. (in Chinese)

基于形状描述符的滞回曲线相似性指标的形成

陈再现　许耀龙

(哈尔滨工业大学(威海)土木工程系, 威海 264209)
(哈尔滨工业大学(威海)山东省高等学校土木工程结构与防灾实验室, 威海 264209)

摘要:为了形成全面的相似度指标以评价滞回曲线的拟合程度,引入了已广泛用于图像特征提取的形状描述符,并提出了基于这些描述符形成计算数值模拟曲线相对于实验曲线的相似度指标的具体流程. 根据该流程,形成了一个基于形状上下文的相似度指标. 先计算两曲线滞回圈之间的相似度,再对这些相似度进行加权组合,形成整个滞回环的相似度. 为了验证该指标,采用 Bouc-Wen 模型进行数值模拟研究. 改变 Bouc-Wen 模型的 5 个参数,并形成 51 条数值模拟曲线,计算这些曲线相对于中值曲线的相似度与力峰值点、耗能、刚度误差. 结果表明,相似度与误差之间的斯皮尔曼相关系数绝对值均大于 0.78,有强烈的相关性,从而验证了该指标的可行性和指标形成流程的有效性.

关键词:滞回曲线; 形状描述符; 形状上下文; Bouc-Wen 模型; 曲线相似性
中图分类号:TU317.1